

# Plasticity-Aware Mixture of Experts for Learning Under QoE Shifts in Adaptive Video Streaming

Zhiqiang He

hezhiqiang@ieee.org

The University of Electro-Communications  
Tokyo, Japan

Zhi Liu\*

liu@ieee.org

The University of Electro-Communications  
Tokyo, Japan

## Abstract

Adaptive video streaming systems are designed to optimize Quality of Experience (QoE) and, in turn, enhance user satisfaction. However, differences in user profiles and video content lead to different weights for QoE factors, resulting in user-specific QoE functions and, thus, varying optimization objectives. This variability poses significant challenges for neural networks, as they often struggle to generalize under evolving targets—a phenomenon known as plasticity loss that prevents conventional models from adapting effectively to changing optimization objectives. To address this limitation, we propose the Plasticity-Aware Mixture of Experts (PA-MoE), a novel learning framework that dynamically modulates network plasticity by balancing memory retention with selective forgetting. In particular, PA-MoE leverages noise injection to promote the selective forgetting of outdated knowledge, thereby endowing neural networks with enhanced adaptive capabilities. In addition, we present a rigorous theoretical analysis of PA-MoE by deriving a regret bound that quantifies its learning performance. Experimental evaluations demonstrate that PA-MoE achieves a 45.5% improvement in QoE over competitive baselines in dynamic streaming environments. Further analysis reveals that the model effectively mitigates plasticity loss by optimizing neuron utilization. Finally, a parameter sensitivity study is performed by injecting varying levels of noise, and the results align closely with our theoretical predictions.

## CCS Concepts

• Information Systems → Multimedia streaming; • Computing methodologies → Sequential decision making.

## Keywords

Plasticity loss, Rate Adaption, Reinforcement Learning, Non-stationary

## ACM Reference Format:

Zhiqiang He and Zhi Liu. 2025. Plasticity-Aware Mixture of Experts for Learning Under QoE Shifts in Adaptive Video Streaming. In . Under Review for ACM Multimedia 2025., 16 pages. <https://doi.org/10.1145/nnnnnnn.nnnnnnn>

\*Corresponding author

Permission to make digital or hard copies of all or part of this work for personal or classroom use is granted without fee provided that copies are not made or distributed for profit or commercial advantage and that copies bear this notice and the full citation on the first page. Copyrights for components of this work owned by others than the author(s) must be honored. Abstracting with credit is permitted. To copy otherwise, or republish, to post on servers or to redistribute to lists, requires prior specific permission and/or a fee. Request permissions from [permissions@acm.org](mailto:permissions@acm.org).

Under Reviewer for ACM MM'25, Dublin, Ireland

© 2025 Copyright held by the owner/author(s). Publication rights licensed to ACM.  
ACM ISBN 978-x-xxxx-xxxx-x/YYYY/MM  
<https://doi.org/10.1145/nnnnnnn.nnnnnnn>

## 1 Introduction

Adaptive video streaming (AVS) has become the foundation of modern multimedia applications. To ensure user satisfaction, major platforms like Netflix and YouTube are continually improving playback quality. This improvement is guided by the concept of Quality of Experience (QoE), which incorporates key factors such as bitrate, buffering time, and latency [47]. Traditionally, AVS systems optimize QoE by dynamically adjusting streaming parameters in response to changes in network conditions, ensuring a smooth viewing experience even with varying bandwidth. However, real-world deployments have shown that network bandwidth is not the only factor affecting QoE [7, 30, 57]. Recent evidence suggests that individual user preferences [46] and important regions within video content [6] also play a role in QoE dynamics, making the optimization objective constantly changing. This presents a significant challenge: the optimization criteria are constantly shifting, requiring adaptive models that can track and respond to these changes in real time. In summary, effectively addressing the AVS optimization problem in the face of dynamically changing QoE requires the development of robust, adaptive algorithms that can balance the demands of network variability and evolving user-centric factors [47].

Classical methods like Model Predictive Control [19] struggle with changing objectives. Existing research on QoE dynamics can be broadly divided into two stages. The first stage focuses on the user level, where factors such as user preferences [46] and regions of interest within the video [6, 14] are taken into account. In this stage, data including watch time, likes, and timestamps are utilized to predict user interests, which then inform the adjustment of QoE parameters [20, 21]. The second stage builds on these predictions to optimize QoE, enabling the streaming system to adapt to dynamically changing user demands [55, 56]. However, two-stage optimization methods encounter several challenges that hinder effective QoE optimization. Inaccuracies in user-level predictions can cascade into subsequent stages, resulting in suboptimal outcomes. Furthermore, their sequential nature, dependence on pre-trained models, and reliance on historical data delay real-time adjustments and updates, while also limiting the ability to generalize when faced with QoE variations beyond the training distribution. Some researchers have even posited that supporting a large number of QoE objectives is inherently infeasible [59]. In this work, we challenge that notion by leveraging a neural network capable of effectively managing a broad spectrum of QoE objectives.

The impact of QoE variations on the optimization objective is evident when considering that different content types have distinct QoE preferences. For instance, while news broadcasts may prioritize stable playback even at lower bitrates, sports events demand

higher frame rates and minimal stuttering for an optimal viewing experience. To address these challenges, we propose a unified, single-policy learning approach that overcomes the limitations of two-stage methods by directly adapting to varying QoE objectives within one framework. Nevertheless, employing a single-stage neural network—where a single set of parameters must rapidly learn and adjust to multiple dynamic objectives—presents a formidable challenge for deep neural network-based AVS optimization. Similar to human neurons [36], neural networks are susceptible to plasticity loss; frequent switching between changing objectives disrupts established representations and hinders the retention of previously acquired knowledge [8]. This degradation in plasticity undermines the model's ability to generalize and efficiently adapt to new QoE shifts, complicating the overall optimization process [15, 22, 31]. Fortunately, existing research demonstrates that Mixture of Experts (MoE) architectures can effectively mitigate this issue by preserving network plasticity through the dynamic allocation of specialized experts for different tasks [50]. Moreover, the injection of noise into neural networks has been shown to counteract plasticity loss and enhance overall performance by improving the model's robustness to shifting objectives [4, 9, 33, 34].

Despite significant advancements, current approaches still have notable limitations in dynamically adapting QoE optimization in AVS. While standard mixture-of-experts (MoE) architectures help mitigate plasticity loss, they lack explicit mechanisms to balance forgetting with retention. This can lead to scenarios where outdated experts retain irrelevant knowledge while over-specialized experts struggle to generalize across new QoE objectives [17, 45]. To address these challenges, we propose Plasticity-Aware Mixture of Experts (PA-MoE), a novel learning framework designed to regulate neural plasticity in response to dynamic QoE shifts. Our approach draws inspiration from human adaptive behavior, where selective suppression of irrelevant memories [3] facilitates adjustment to changing environments. PA-MoE integrates a controlled forgetting mechanism via noise injection [34], systematically discarding obsolete knowledge while preserving essential shared information through adaptive weight adjustments. By striking an optimal balance between adaptability and stability, PA-MoE ensures efficient learning and robust performance across a wide range of QoE optimization objectives in AVS. Furthermore, our approach is supported by a rigorous theoretical analysis that substantiates its efficacy.

In summary, this paper makes the following contributions:

- **Novel Problem Analysis:** We are the first to identify the loss of neural network plasticity induced by fluctuations in QoE, providing a new perspective on optimizing systems for shifts in QoE due to changes in user preferences and video content.
- **Algorithm Design:** We propose PA-MoE, a novel algorithm that incorporates controlled noise injection into experts to actively eliminate outdated knowledge, thus maintaining the adaptive capability of the MoE framework.
- **Theoretical Foundation:** We provide a rigorous theoretical analysis of PA-MoE by deriving its performance regret bound and demonstrating how noise injection dynamically balances the trade-off between forgetting and memory retention.
- **Implementation and Evaluation:** Extensive experiments show that PA-MoE rapidly adapts to QoE shifts, achieving a 45.5%

performance improvement over conventional MoE models. Comprehensive analysis across multiple metrics elucidates the mechanisms behind PA-MoE's effectiveness in adapting to dynamic system changes, while a sensitivity study on noise injection further validates our theoretical framework.

## 2 Background And Motivation

### 2.1 Problem Formulation

In adaptive video streaming [18], a video is typically divided into  $I$  consecutive chunks  $\{V_1, V_2, \dots, V_I\}$ , with each chunk lasting  $t_i$  seconds. These chunks are encoded at multiple bitrates  $b \in \mathbb{B} = \{b_1, b_2, \dots, b_J\}$  in ascending order, such that the size of chunk  $i$ , denoted as  $d_i^b$ , increases with the bitrate  $b$ . The goal is for a reinforcement learning agent to select the optimal bitrate for each chunk in order to maximize QoE. To prevent interruptions during transitions between segments  $V_i$  and  $V_{i+1}$ , a playback buffer  $B_f$  is used to prefetch upcoming segments, allowing for simultaneous playback and downloading. The buffer occupancy,  $B_f(t)$ , is limited to the interval  $[0, B_f^{max}]$  to account for server or client limitations.

The download time for segment  $V_i^b$  is composed of two main components: the network round-trip time  $t_{RTT}$  and data transfer time  $d_i^b/S_i$  represents the download speed. In order to account for network variability, a noise factor  $\eta(i)$  is introduced. As a result, the download start time for segment  $V_{i+1}$  can be calculated as  $t_{i+1}^d = t_i^d + \left(\frac{d_i^b}{S_i} + t_{RTT}\right) \times \eta(i) + \Delta t_i^w$ , where  $\Delta t_i^w$  is a deliberate waiting period implemented to manage buffer constraints. The evolution of buffer occupancy is described by:

$$B_f(t_{i+1}) = \left( (B_f(t_i) - t_{\text{delay}})_+ + t_i - \Delta t_i^w \right)_+, \quad (1)$$

with the network delay defined as  $t_{\text{delay}} = \left(\frac{d_i^b}{S_i} + t_{RTT}\right) \times \eta(i)$ . To prevent buffer overflow, the waiting time is determined by

$$\Delta t_i^w = \left( (B_f(t_i) - t_{\text{delay}})_+ + t_i - B_f^{max} \right)_+. \quad (2)$$

In adaptive video streaming, the central objective is to optimize the QoE. A typical QoE model incorporates three critical components. The first component is the **BitRate** factor, which measures the average video quality, given by  $\frac{1}{I} \sum_{i=1}^I q(V_i^b)$ , where  $q(\cdot)$  is a monotonically increasing quality function; The second component is the **Smooth** factor, which penalizes quality fluctuations. This is represented by the term  $\frac{1}{I-1} \sum_{i=1}^{I-1} |q(V_{i+1}^b) - q(V_i^b)|$ . This captures the perceptual impact of abrupt changes in quality. The third component is the **Rebuffer** penalty, which accounts for playback interruptions due to buffer underruns caused by network delays and transmission time. These factors are combined into a weighted sum to balance video quality, smoothness, and playback stability:

$$\begin{aligned} QoE^I = & \mu_1 \sum_{i=1}^I q(V_i^b) - \mu_2 \sum_{i=1}^{I-1} |q(V_{i+1}^b) - q(V_i^b)| \\ & - \mu_3 \sum_{i=1}^I \left( \left( \frac{d_i(V_i^b)}{S_i} + t_{RTT} \right) \times \eta(i) - B_f(t_i) \right)_+. \end{aligned} \quad (3)$$

Accordingly, the overall problem is naturally formulated as a sequential decision-making process, which can be modeled as a Markov Decision Process (MDP). This formulation enables the application of state-of-the-art reinforcement learning algorithms to effectively address the QoE optimization challenge in adaptive video streaming.

## 2.2 Markov Decision Process With Shift QoE

An MDP is formally defined as a tuple  $(S, \mathcal{A}, \mathcal{P}, \mathcal{R}, \gamma)$ , where  $S$  represents the state space containing all the pertinent information for decision-making, and  $\mathcal{A}$  denotes the action space comprising all feasible decisions. The transition function  $\mathcal{P} : S \times \mathcal{A} \rightarrow \Delta(S)$  captures the stochastic evolution of states, while the reward function  $\mathcal{R} : S \times \mathcal{A} \rightarrow \mathbb{R}$  delivers QoE-aligned feedback to guide the learning process. The discount factor  $\gamma \in [0, 1)$  is employed to balance short-term and long-term rewards.

In our formulation, the state space  $S$  includes important streaming indicators such as the quality of the last downloaded chunk, buffer occupancy, network throughput and delay, sizes of upcoming chunks, and the number of remaining chunks. This comprehensive representation allows the agent to make informed decisions based on the context. The action space  $\mathcal{A}$  consists of multiple discrete bitrate levels, each corresponding to a different quality version. Lastly, the reward  $\mathcal{R}$  is directly determined by the QoE metric, effectively balancing the trade-offs between video quality, smoothness, and playback stability.

By utilizing reinforcement learning (RL), the system is able to adaptively learn optimal control strategies, even in uncertain environments. This effectively addresses the challenges posed by dynamic and unpredictable system behavior. However, when there are shifts in QoE due to variations in video content, the reward function experiences significant changes across the state space. This variability transforms the problem into a non-stationary MDP, which can be seen as a sequence of distinct MDPs  $\{M_1, M_2, \dots, M_N\}$ . Each MDP  $M_n = (S, \mathcal{A}, \mathcal{P}, \mathcal{R}_n, \gamma)$  represents a unique optimization problem defined by its own reward structure. This non-stationarity poses a fundamental challenge for conventional learning algorithms, as policies optimized for one network environment may fail catastrophically when deployed in another. Therefore, there is a critical need for adaptive strategies that can generalize across these dynamic and evolving conditions.

## 2.3 Impact of Shift QoE on RL

To demonstrate the impact of QoE shifts on reinforcement learning-based optimization and the resulting loss of neural plasticity, we conducted an experimental case study. Specifically, we designed three distinct video types—documentaries (D,  $\{\mu_1 = 1, \mu_2 = 6, \mu_3 = 1\}$ ), live streams (L,  $\{\mu_1 = 1, \mu_2 = 1, \mu_3 = 6\}$ ), and news (N,  $\{\mu_1 = 6, \mu_2 = 1, \mu_3 = 1\}$ )—each with different coefficients for the QoE components in our system model. Figure 1 illustrates the action outputs of reinforcement learning agents using the Proximal Policy Optimization (PPO) [40] algorithm across various network architectures as the system conditions evolve.

This example highlights the impact of changes in QoE parameters on the adaptability of learning agents. Specifically, agents using a multilayer perceptron (MLP) architecture struggle to quickly adjust

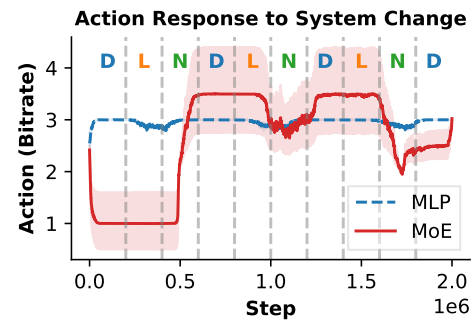


**Figure 1: Action output variation across different network architectures under shifted QoE reward conditions. D, L, and N represent distinct QoE metrics. An ideal agent adapts its actions as QoE changes, but the adaptability varies with network design.**

their actions in response to QoE changes, while those utilizing a mixture-of-experts (MoE) architecture show a much stronger ability to adapt to evolving QoE. However, the changes in actions do not follow a clear pattern that directly corresponds to the periodic shifts in QoE.

## 3 Related Work

We evaluate PA-MoE in comparison with related approaches along three key dimensions: adaptive video streaming under varying QoE metrics, MDP adaptation and optimization in video streaming, and the application of Mixture of Experts methods in policy learning.

### 3.1 Content Aware Video Streaming

QoE metrics are broadly classified into pixel-based quality and streaming quality [7]. Pixel-based quality evaluates intrinsic visual fidelity—such as sharpness, color accuracy, and contrast—independently of network-induced distortions, whereas streaming quality encompasses dynamic factors including playback smoothness, quality degradation, buffering frequency, and user-specific sensitivity to quality variations [55]. In this work, we concentrate on QoE variations driven by streaming quality.

Conventional approaches typically estimate QoE by inferring users’ regions of interest within a video [14]. Some methods utilize deep learning models, such as CNNs and Transformers [6], while others rely on engagement signals, such as timestamps, likes, and watch duration, to approximate user preferences [20]. However, prior studies have primarily focused on modeling QoE variations within a single video type. In contrast, our study investigates QoE shifts across different video types [27], providing a broader perspective on adaptive streaming optimization.

Once user-preference-aware QoE is estimated, traditional techniques optimize adaptive streaming through buffer-based strategies [20, 21], reinforcement learning [46, 59], apprenticeship learning [27], or user-specific models [56]. These two-stage optimization methods introduce additional computational overhead, and the performance of the first stage does not have a clear correlation with the overall performance [16]. In this paper, we propose a unified

policy that dynamically modulates network memory and plasticity through noise injection, thereby enabling rapid adaptation to evolving QoE patterns.

### 3.2 Video Streaming with QoE Shifts

If a single policy is used to handle multiple MDPs simultaneously, it falls under the category of Multi-Task Learning (MTL) [51]. On the other hand, training a policy in a streaming manner to adapt to continuously changing MDPs is classified as Continual Learning [1]. For example, concurrently training a policy to handle  $M_1$  and  $M_2$  would be considered to MTL, while training sequentially on  $M_1$  for a set number of steps, then on  $M_2$  and cycling through (e.g.,  $M_1 \rightarrow M_2 \rightarrow M_1 \rightarrow M_2$ ) would be classified as Continual Learning. In our work, we focus on streaming tasks that involve dynamic QoE shifts in video streaming, which can be modeled as a sequence of MDPs (e.g.,  $M_1 \rightarrow M_2 \rightarrow \dots, \rightarrow M_1 \rightarrow \dots$ ) [11].

Modeling system changes as a Continual Learning problem is a common approach [54]. However, existing methods typically decompose the challenge. For example, some methods first employ a monitor to detect system changes before applying adjustments such as retraining [54], while others use meta-reinforcement learning. Meta reinforcement learning enables systems to "learn how to learn" across multiple tasks [28, 49], facilitating rapid adaptation. However, this approach often assumes that tasks share certain stationary properties in their distributions, which is often unrealistic in real-world adaptive video streaming applications.

In contrast, our approach does not rely on a two-stage optimization or require prior knowledge of task relationships or distributions. Instead, we directly adjust the plasticity of neural networks through noise injection, enabling them to dynamically adapt to varying optimization objectives based on the data.

### 3.3 Mixture of Experts

The MoE architectures utilizes a router mechanism to dynamically assign input states to specialized expert networks for decision-making [5]. This approach has been widely adopted in large-scale models [26, 29, 52] and has shown exceptional performance in multi-task learning and Continual Learning (CL) scenarios [25]. However, a key challenge in MoE is effectively allocating tasks to experts. To address this, various strategies have been explored, including linear programming [23], reinforcement learning [38], optimal transport [48], and greedy top-k token selection [58]. Recent advancements, such as Soft MoE, have introduced slot-based connectivity to allow for more flexible integration of experts [37]. Other approaches have also explored parameter composition to optimize task-specific expert selection [45]. In our video streaming task, even the basic Sparse MoE (SMoE) can efficiently allocate tasks to achieve load balancing. To better investigate the problem and eliminate the influence of other factors, we opted for the simplest form of SMoE [42].

Our approach differs from existing strategies that primarily aim to reduce computational overhead during inference. Instead, we focus on enhancing MoE adaptability, which is crucial for real-world applications where the policy network needs to quickly adjust to new tasks. To achieve this, we introduce a knowledge forgetting module that selectively discards outdated information to preserve

plasticity. Additionally, our memory mechanism allows the neural network to autonomously adjust its weights, effectively counterbalancing the effects of active forgetting. Previous research has mainly focused on knowledge sharing, but methods such as direct parameter copying or weight sharing can result in negative transfer, as not all information is beneficial to share [17]. In contrast, our approach exclusively injects forgetting, giving the network the ability to independently retain valuable memories.

Moreover, recent studies have shown that RL policy networks often have a significant number of underutilized parameters, with around 90% of neuron outputs remaining inactive [44]. Injecting noise into network parameters has found to be effective in maintaining plasticity and improving overall performance [10, 41, 44]. While noise perturbations are commonly used in traditional dense architectures [34, 35], our work maintains the plasticity of MoE models by injecting noise into the gradients. Additionally, we provide a theoretical analysis of the regret bound associated with our proposed PA-MoE method to support our approach.

## 4 Proposed Method

### 4.1 Architectural Paradigm of the MoE Framework

The challenge posed by QoE shifts is that they render the underlying problem non-stationary, leading to a loss of agent plasticity and hindering rapid adaptation for dynamic knowledge transfer [17, 45]. In order to address these issues, we propose the PA-MoE method, which directly injects plasticity into the experts of the MoE architecture. In a typical MoE model, there are  $N$  experts, a router, and a gating network—usually implemented as a series of linear layers [12].

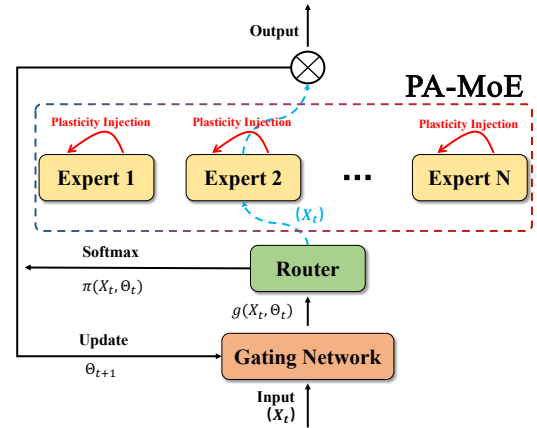


Figure 2: An illustration of the PA-MoE model.

The framework of PA-MoE is illustrated in Figure 2. Once the MDP is formulated, the next step is to identify a mapping from input states to actions, known as the policy. At time step  $t$ , the input state vector is denoted by  $X_t \in \mathbb{R}^d$ . The gating network applies a linear transformation to  $X_t$ , producing an output  $g_n(X_t, \mathbf{w}_t^{(n)})$  for each expert  $n \in [N]$ , where  $\mathbf{w}_t^{(n)} \in \mathbb{R}^n$  represents the parameters

corresponding to expert  $n$ . The complete set of gating network parameters is represented as  $\mathbf{w}_t := [\mathbf{w}_t^1, \dots, \mathbf{w}_t^{(N)}]$ , and the overall gating output is defined as

$$\mathbf{g}(X_t, \mathbf{w}_t) := [g_1(X_t, \mathbf{w}_t^{(1)}), \dots, g_N(X_t, \mathbf{w}_t^{(N)})], \quad (4)$$

which can equivalently be expressed as  $\mathbf{g}(X_t, \mathbf{w}_t) = \mathbf{w}_t^T X_t$ . To enhance network sparsity and reduce computational costs, our router selects only the Top-1 expert—that is, the expert corresponding to the maximum gating output—as demonstrated in [12, 24]. Furthermore, to promote exploration, noise is injected into the router following the methods outlined in [12, 25]. Specifically, the chosen expert at time step  $t$  is determined by

$$n_t = \arg \max_n \left\{ g_n(X_t, \mathbf{w}_t^{(n)}) + z_t^{(n)} \right\}, \quad (5)$$

where  $z_t^{(n)}$  is a noise term drawn from a Gaussian distribution for each expert  $n$ . This stochastic component promotes exploration by perturbing the gating output. Furthermore, the final output of the gating network is computed using a softmax function:

$$\pi_n(X_t, \mathbf{w}_t) = \frac{\exp(g_n(X_t, \mathbf{w}_t^{(n)}))}{\sum_{n'=1}^N \exp(g_{n'}(X_t, \mathbf{w}_t^{(n')}))}, \quad \forall n \in [N], \quad (6)$$

This softmax output represents a probability distribution over the experts and is subsequently used to update the gating network parameters  $\mathbf{w}_{t+1}$  for all experts in the MoE model.

## 4.2 Training Expert With Plasticity Injection

In this section, we will introduce the PA-MoE method for plasticity injection. Random perturbations and resets of neural network parameters have been shown to be effective strategies for mitigating plasticity loss in reinforcement learning [13, 43]. In our PA-MoE framework, we enhance plasticity by injecting controlled noise directly into the parameter updates. To validate the effectiveness of this approach, we integrate it into a state-of-the-art reinforcement learning algorithm, PPO.

Let  $\mathbf{w}_t^{(n)}$  denote the parameters of expert  $n$  in the actor network at the  $t$ -th training step. The policy distribution at time step  $t$  is then given by:

$$\pi_{\mathbf{w}}(a_t | X_t) = \sum_{n=1}^N \pi_n(X_t, \mathbf{w}_t) \mathbf{w}_t^{(n)}(X_t). \quad (7)$$

For the critic, the update rule is defined as:

$$L^{critic}(\mathbf{w}) = \mathbb{E}_t \left[ \left( V_{\mathbf{w}}(X_t) - \hat{V}_t \right)^2 \right], \quad (8)$$

where,  $\hat{V}_t$  represents the target value, typically computed using Generalized Advantage Estimation (GAE,  $\hat{A}_t$ ) or a Temporal Difference (TD) target. PPO further employs a clipped surrogate objective defined as

$$L_t(\mathbf{w}) = \mathbb{E}_t \left[ \min \left( r_t(\mathbf{w}) \hat{A}_t, \text{clip} \left( r_t(\mathbf{w}), 1 - \epsilon, 1 + \epsilon \right) \hat{A}_t \right) \right], \quad (9)$$

with the probability ratio

$$r_t(\mathbf{w}) = \pi_{\mathbf{w}}(a_t | s_t) / \pi_{\mathbf{w}_{old}}(a_t | s_t). \quad (10)$$

For each normal expert  $i$  (selected via the Top-K mechanism), we perform a noisy gradient descent update. Specifically, the update at time  $t$  is given by

$$\mathbf{w}_i^{t+1} = \mathbf{w}_i^t - \eta \nabla L_t(\mathbf{w}_i^t) + \eta \gamma \epsilon_i^t, \quad t = 1, 2, \dots, T, \quad (11)$$

where  $\eta > 0$  is the learning rate, assumed to satisfy  $\eta \leq 1/L$ ,  $\gamma > 0$  controls the noise injection strength, and  $\epsilon_i^t \sim \mathcal{N}(0, I_d)$  is a standard Gaussian noise vector in  $\mathbb{R}^d$ , independent across time steps and experts. This noise injection facilitates a form of controlled forgetting by discarding outdated information, thereby enhancing the model's ability to adapt to nonstationary environments. We provide a theoretical analysis of this mechanism below.

In PPO, the policy update is constrained within a trust region, which ensures that each update only makes small changes to the current parameters. Although the global objective may be highly nonconvex, within the trust region, the loss function can be well approximated locally by a quadratic function. This approximation allows us to make certain assumptions about the behavior of the loss function, such as being  $L$ -smooth and  $\mu$ -strongly convex, which are useful for theoretical analysis and understanding how the parameters adapt to a changing environment.

Let  $L_t(\mathbf{w})$ , with  $\mathbf{w} \in \mathbb{R}^d$ , denote each expert's local objective at time  $t$ . We consider the following standard assumptions:

**(A1)  $L$ -Smoothness:** For all  $\mathbf{w}, \mathbf{w}' \in \mathbb{R}^d$ , the gradient of  $L_t$  is Lipschitz continuous,  $\|\nabla L_t(\mathbf{w}) - \nabla L_t(\mathbf{w}')\| \leq L \|\mathbf{w} - \mathbf{w}'\|$ , where  $L > 0$  is the smoothness constant.

**(A2)  $\mu$ -Strong Convexity:** For all  $\mathbf{w}, \mathbf{w}' \in \mathbb{R}^d$ , the function  $L_t$  satisfies,  $L_t(\mathbf{w}') \geq L_t(\mathbf{w}) + \nabla L_t(\mathbf{w})^T (\mathbf{w}' - \mathbf{w}) + \frac{\mu}{2} \|\mathbf{w}' - \mathbf{w}\|^2$ , with  $\mu > 0$  being the strong convexity constant.

**(A3) Nonstationarity:** Let the time-varying optimal parameter be defined as  $\mathbf{w}_t^* = \arg \min_{\mathbf{w}} L_t(\mathbf{w})$ . Define the path length of the optimal parameters over  $T$  rounds as  $P_T = \sum_{t=1}^{T-1} \|\mathbf{w}_{t+1}^* - \mathbf{w}_t^*\|$ . We assume that  $P_T < \infty$ ; this quantity measures the rate at which the environment (or the optimum) changes over time.

We now state two key lemmas that are instrumental for our analysis.

**LEMMA 4.1 (GRADIENT CO-COERCIVITY LEMMA).** *Let  $L_t : \mathbb{R}^d \rightarrow \mathbb{R}$  be an  $L$ -smooth function; that is, for all  $\mathbf{w}, \mathbf{w}' \in \mathbb{R}^d$ ,*

$$\|\nabla L_t(\mathbf{w}) - \nabla L_t(\mathbf{w}')\| \leq L \|\mathbf{w} - \mathbf{w}'\|.$$

*Then, for any  $\mathbf{w}_i^t, \mathbf{w}_i^* \in \mathbb{R}^d$ , we have*

$$\begin{aligned} \|\nabla L_t(\mathbf{w}_i^t) - \nabla L_t(\mathbf{w}_i^*)\|^2 & \\ & \leq L (\nabla L_t(\mathbf{w}_i^t) - \nabla L_t(\mathbf{w}_i^*))^T (\mathbf{w}_i^t - \mathbf{w}_i^*). \end{aligned} \quad (12)$$

**PROOF.** See Appendix A.  $\square$

**LEMMA 4.2 (GRADIENT STRONG CONVEXITY LEMMA).** *Let  $L_t : \mathbb{R}^d \rightarrow \mathbb{R}$  be a  $\mu$ -strongly convex function; that is, for all  $\mathbf{w}, \mathbf{w}' \in \mathbb{R}^d$ ,*

$$L_t(\mathbf{w}') \geq L_t(\mathbf{w}) + \nabla L_t(\mathbf{w})^T (\mathbf{w}' - \mathbf{w}) + \frac{\mu}{2} \|\mathbf{w}' - \mathbf{w}\|^2.$$

Then, for any  $\mathbf{w}_i^t, \mathbf{w}_i^* \in \mathbb{R}^d$ , it holds that

$$(\nabla L_t(\mathbf{w}_i^t) - \nabla L_t(\mathbf{w}_i^*))^T (\mathbf{w}_i^t - \mathbf{w}_i^*) \geq \mu \|\mathbf{w}_i^t - \mathbf{w}_i^*\|^2. \quad (13)$$

PROOF. See Appendix B.  $\square$

**THEOREM 4.3 (TRACKING ERROR BOUND UNDER NONSTATIONARITY).** Under Assumptions (A1)–(A3) and with the update rule

$$\mathbf{w}_i^{t+1} = \mathbf{w}_i^t - \eta \nabla L_t(\mathbf{w}_i^t) + \eta \gamma \epsilon_i^t, \quad \epsilon_i^t \sim \mathcal{N}(0, I_d), \quad (14)$$

there exists a constant  $C > 0$  (depending only on  $L$  and  $\mu$ ) such that the average squared error satisfies

$$\frac{1}{T} \sum_{t=1}^T \mathbb{E} \|e_t\|^2 \leq C \left( \eta \gamma^2 d + \frac{P_T^2}{T\eta} \right), \quad (15)$$

where the error is defined as  $e_t = \mathbf{w}_i^t - \mathbf{w}_i^*$  and the path length of the optimal parameters is  $P_T = \sum_{t=1}^{T-1} \|\mathbf{w}_{i+1}^* - \mathbf{w}_i^*\|$ .

PROOF. See Appendix C.  $\square$

We will now analyze Theorem 4.3 from the perspectives of active forgetting and memorization. **Active Forgetting:** The term  $\eta \gamma^2 d$  in the error bound increases linearly with the learning rate  $\eta$ . A higher  $\eta$  implies that each expert updates its parameters more aggressively in response to new information, effectively promoting active forgetting - rapidly discarding outdated information in favor of recent data. However, if  $\eta$  is set too high, the amplified noise (scaled by  $\gamma$ ) can render the updates overly volatile, potentially destabilizing the model. Therefore, while a larger  $\eta$  facilitates swift adaptation, it must be chosen carefully to avoid excessive noise-induced fluctuations. **Memorization:** On the other hand, the term  $\frac{P_T^2}{T\eta}$  is inversely proportional to  $\eta$ . This means that a smaller  $\eta$  will result in slower updates of the parameter, causing the model to hold onto outdated information. This can be thought of as the model "memorizing" past data. However, this excessive retention hampers the expert's ability to track the current optimal parameters, particularly when the environment is nonstationary and the optimum drifts over time (as captured by the path length  $P_T$ ). Therefore, an overly small  $\eta$  results in insufficient active forgetting, leading to larger tracking errors.

In summary, excessive noise can cause the neural network's updates to be overly influenced by the noise, resulting in a biased model that is prone to forgetting. Conversely, insufficient noise can lead to the updates be dominated by  $\frac{P_T^2}{T\eta}$ , causing outdated information to become fixed in the model. Therefore, it is crucial to properly control both the noise level and the learning rate. This requires striking a balance between having a large enough noise level to actively forget outdated information and adapt to new conditions, while also keeping the noise-induced error under control.

## 5 Experiments

In our experiments, we aim to address the following key questions from three perspectives: **Cause, Effect, and Analysis:** (1.1) Can PA-MoE effectively mitigate the problem of plasticity loss? (1.2) Do different experts in PA-MoE contribute to alleviating plasticity loss? (1.3) Is the selection probability of each expert in PA-MoE balanced? (2.1) Does PA-MoE offer performance improvements compared to

the vanilla MoE architecture? (2.2) How do individual components of QoE contribute to the overall performance gains observed in PA-MoE? (2.3) How does PA-MoE influence internal system states to ultimately affect performance? (3) What is the impact of the injected noise scale on the final performance of PA-MoE?

### 5.1 Experiment Setting

The experimental setup and hyperparameter configurations are provided in Appendix D. All hyperparameters, including random seeds, are kept consistent across different algorithms. All code and data will be open-sourced upon paper acceptance. All QoE shift patterns in this paper follow the format illustrated in Figure 1.

### 5.2 Does PA-MoE alleviate the issue of plasticity loss?

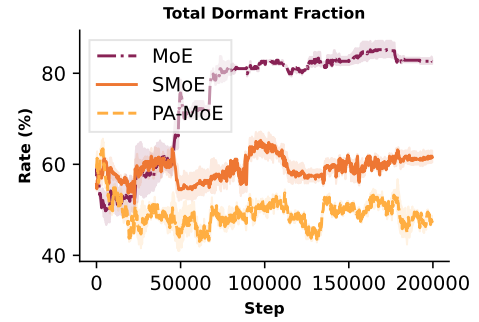


Figure 3: Evolution of neural network dormant neuron rate.

A neuron that does not contribute to subsequent layers is known as a Dormant Neuron (for a detailed definition, see Appendix E). The dormant neuron ratio is a widely adopted metric for evaluating neural network plasticity [8, 44, 51]. Figure 3 illustrates the evolution of dormant neuron ratios under QoE shifts across various network architectures. Our proposed PA-MoE consistently maintains a lower dormant neuron ratio compared to both Sparse MoE (SMoE) and conventional MoE, and this ratio does not exhibit an increasing trend over time.

To determine if different experts in PA-MoE contribute to mitigating plasticity loss, we visualize the dormant neuron ratios for each layer in the policy and value networks of every expert (see Appendix E). These visualizations demonstrate that PA-MoE consistently exhibits lower dormant neuron ratios across various layers in both the policy and value networks when compared to conventional MoE and SMoE.

Another widely used metric for characterizing the loss of learning capacity in neural networks is Feature Rank [8, 31]. In Appendices F, G, H, and I, we show that our PA-MoE method achieves higher effective rank [39], approximate rank, and absolute approximate rank [53] compared to other approaches. These results indicate that PA-MoE preserves a stronger learning capacity with significantly reduced plasticity loss.

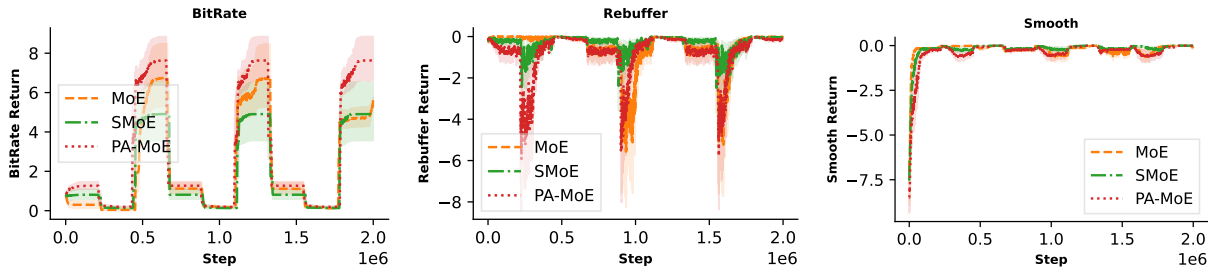


Figure 4: Performance Comparison of Different Algorithms Based on QoE Component Metrics

### 5.3 Are the selection probabilities for each expert balanced?

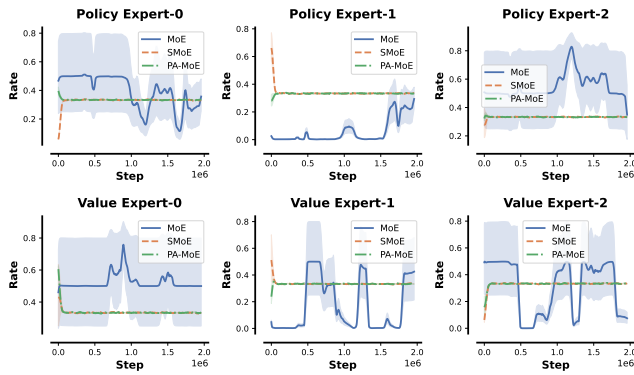


Figure 5: Probability distribution of each expert selected for Policy and Value.

Load balancing is a critical factor in evaluating the effectiveness of MoE designs. In a load-balanced MoE, all experts are utilized evenly, preventing some experts from being overused while others remain idle. This leads to improved computational efficiency. Additionally, a balanced allocation promotes diverse feature learning among experts, ultimately enhancing the model’s ability to handle complex tasks. To validate the load-balancing capability of our proposed PA-MoE, we visualized the selection probability of each expert in both the policy and value functions. As shown in Figure 5, our experimental results clearly demonstrate that each expert in PA-MoE is selected with equal probability. This balanced selection effectively avoids over-reliance on a subset of experts, thereby reducing the risk of overfitting and ensuring robust performance across diverse tasks.

### 5.4 Does PA-MoE Yield Performance Improvements?

Another question that we are interested in is: Does PA-MoE result in performance improvements? Additionally, we would like to understand how the individual components of QoE contribute to the overall QoE under Shift QoE conditions. The variation curve of the overall QoE in a Shift QoE environment is depicted in Figure 6.

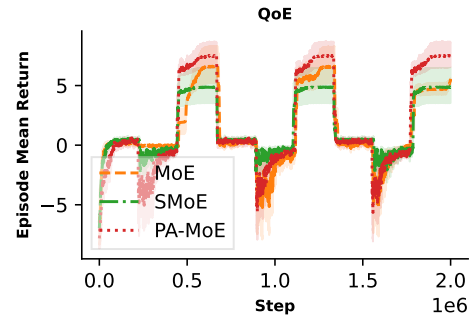


Figure 6: Final QoE Performance Comparison of Different Algorithms under Shift QoE.

As illustrated in Figure 6, it is clear that MoE requires a great number of steps to generate enough interaction data to adapt to the changing QoE, while PA-MoE quickly adapts and achieves higher performance gains. To more accurately measure these improvements, we utilize the more reliable reinforcement learning metric, the IQM (Interquartile Mean) [2], as shown in Figure 7. This method aims to emphasize the relative performance of different approaches while reducing the influence of outliers.

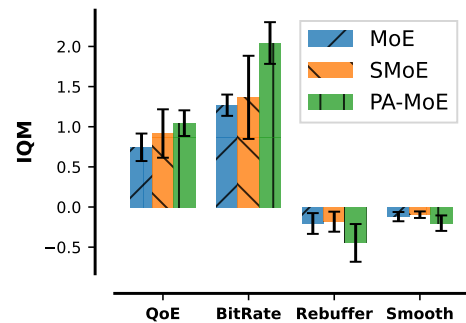
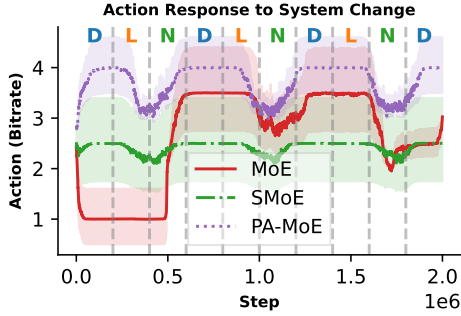


Figure 7: Comparison of QoE Methods using the IQM with a focus on the 25th-75th percentile returns.

The results shown in Figure 7 demonstrate that our PA-MoE method improves overall QoE by 45.5% compared to conventional MoE. The most significant improvements are seen in the Bitrate

component, indicating that the agent is able to selectively optimize the different QoE components to meet the requirements of a Shift QoE environment. More detailed changes for each metric can be seen in Figure 4.

### 5.5 Influence on System Internal States



**Figure 8: Illustration of Internal State Metrics Variations in a Video Streaming System under Shift QoE Conditions.**

In this section, we present visualizations of the system’s internal state metrics to analyze the behavior of different algorithms. This will help us gain a better understanding of their impact on overall QoE. As shown in Figure 8, we can see that PA-MoE exhibits periodic variations in the action space, which correspond to system changes. On the other hand, SMoE only shows minor fluctuations and fails to adapt quickly. In contrast, MoE does not demonstrate any periodic adaptation. Furthermore, Figure 9 illustrates detailed variations across the entire internal state of the system, revealing that PA-MoE more effectively utilizes the buffer size, resulting in higher throughput.

### 5.6 Noise Sensitivity Analysis in PA-MoE

In PA-MoE, the magnitude of noise injection is a critical parameter. Our sensitivity analysis, presented in Figure 10, reveals that both excessively low and high noise levels lead to performance degradation. This observation aligns with our theoretical analysis and validates Theorem 4.3. Furthermore, as shown in Appendix J, visualizations of the weight magnitudes indicate that the neural network adaptively adjusts its weights to retain memory and counteract noise-induced forgetting. These findings underscore the importance of carefully tuning the noise level to balance plasticity and stability in dynamic environments.

## 6 Conclusion

In this paper, we revisit the paradigm of optimization under changing objective functions in adaptive video streaming. We introduce PA-MoE, a novel approach designed to mitigate neural network plasticity loss during the optimization process under dynamic QoE shift scenarios. Our method leverages controlled noise injection to enable robust and rapid adaptation. We provide rigorous theoretical insights and analysis to support the effectiveness of PA-MoE, and extensive experiments validate both the identified problem and

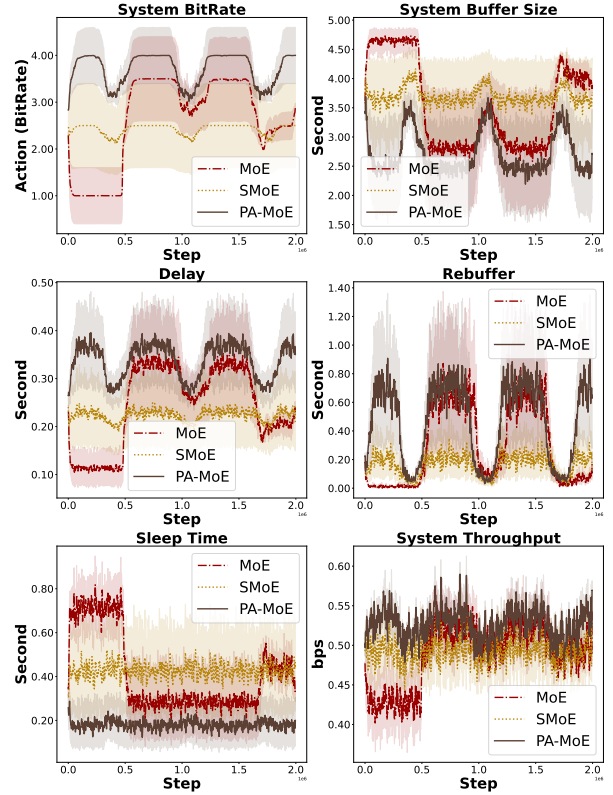


**Figure 9: Variations in the Internal State Metrics of the Video Streaming System.**

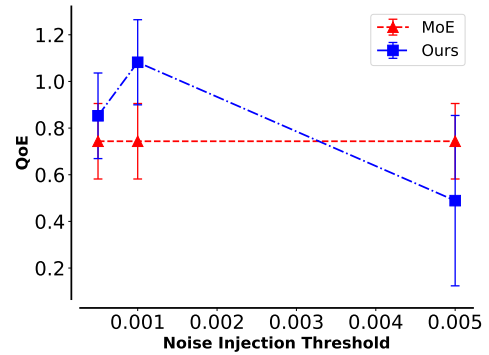


**Figure 10: Comparison of QoE Methods using the IQM (Interquartile Mean) with a focus on the 25th-75th percentile returns. This approach aims to highlight the relative performance of different methods while minimizing the impact of outliers.**

our proposed solution from multiple perspectives. Additionally, parameter sensitivity studies further corroborate our theoretical claims. Future work may explore more advanced strategies for alleviating plasticity loss, building on the foundational noise injection mechanism presented here.

## References

- [1] Zaheer Abbas, Rosie Zhao, Joseph Modayil, Adam White, and Marlos C. Machado. 2023. Loss of Plasticity in Continual Deep Reinforcement Learning. In *CoLLAs (Proceedings of Machine Learning Research, Vol. 232)*. PMLR, 620–636. <http://dblp.uni-trier.de/db/conf/collas/collas2023.html#AbbasZM0M23>
- [2] Rishabh Agarwal, Max Schwarzer, Pablo Samuel Castro, Aaron C Courville, and Marc Bellemare. 2021. Deep reinforcement learning at the edge of the statistical precipice. *Advances in neural information processing systems* 34 (2021), 29304–29320.
- [3] Michael C Anderson and Collin Green. 2001. Suppressing unwanted memories by executive control. *Nature* 410, 6826 (2001), 366–369.
- [4] Jordan Ash and Ryan P Adams. 2020. On warm-starting neural network training. *Advances in neural information processing systems* 33 (2020), 3884–3894.
- [5] Weilin Cai, Juyong Jiang, Fan Wang, Jing Tang, Sunghun Kim, and Jiayi Huang. 2024. A survey on mixture of experts. *arXiv preprint arXiv:2407.06204* (2024).
- [6] Wangyu Choi and Jongwon Yoon. 2024. Data-Driven Video Scene Importance Estimation for Adaptive Video Streaming. In *2024 Fifteenth International Conference on Ubiquitous and Future Networks (ICUFN)*. IEEE, 348–351.
- [7] Florin Dobrian, Vyas Sekar, Asad Awan, Ion Stoica, Dilip Joseph, Aditya Ganjam, Jibin Zhan, and Hui Zhang. 2011. Understanding the impact of video quality on user engagement. *ACM SIGCOMM computer communication review* 41, 4 (2011), 362–373.
- [8] Shibhansh Dohare, J Fernando Hernandez-Garcia, Qingfeng Lan, Parash Rahman, A Rupam Mahmood, and Richard S Sutton. 2024. Loss of plasticity in deep continual learning. *Nature* 632, 8026 (2024), 768–774.
- [9] Pierluca D’Oro, Max Schwarzer, Evgenii Nikishin, Pierre-Luc Bacon, Marc G Bellemare, and Aaron Courville. 2022. Sample-efficient reinforcement learning by breaking the replay ratio barrier. In *Deep Reinforcement Learning Workshop NeurIPS 2022*.
- [10] Pierluca D’Oro, Max Schwarzer, Evgenii Nikishin, Pierre-Luc Bacon, Marc G Bellemare, and Aaron Courville. 2023. Sample-Efficient Reinforcement Learning by Breaking the Replay Ratio Barrier. In *The Eleventh International Conference on Learning Representations*. <https://openreview.net/forum?id=OpC-9aBBVJc>
- [11] Mohamed Elsayed, Gautham Vasan, and A Rupam Mahmood. 2024. Streaming Deep Reinforcement Learning Finally Works. *arXiv preprint arXiv:2410.14606* (2024).
- [12] William Fedus, Barret Zoph, and Noam Shazeer. 2022. Switch transformers: Scaling to trillion parameter models with simple and efficient sparsity. *Journal of Machine Learning Research* 23, 120 (2022), 1–39.
- [13] Alexandre Galashov, Michalis Titsias, András György, Clare Lyle, Razvan Pascanu, Yee Whye Teh, and Maneesh Sahani. 2024. Non-Stationary Learning of Neural Networks with Automatic Soft Parameter Reset. In *The Thirty-eighth Annual Conference on Neural Information Processing Systems*. <https://openreview.net/forum?id=fDiZJ7mmOV>
- [14] Guanyu Gao, Linsen Dong, Huaizheng Zhang, Yonggang Wen, and Wenjun Zeng. 2019. Content-Aware Personalised Rate Adaptation for Adaptive Streaming via Deep Video Analysis. In *ICC 2019 - 2019 IEEE International Conference on Communications (ICC)*. 1–8. <https://doi.org/10.1109/ICC.2019.8761156>
- [15] Caglar Gulchhre, Srivatsan Srinivasan, Jakub Sygnowski, Georg Ostrovski, Mehrdad Farajtabar, Matthew Hoffman, Razvan Pascanu, and Arnaud Doucet. 2022. An empirical study of implicit regularization in deep offline RL. *Transactions on Machine Learning Research* (2022). <https://openreview.net/forum?id=HFfJWx60IT>
- [16] Zhiqiang He, Wen Qiu, Wei Zhao, Xun Shao, and Zhi Liu. 2025. Understanding world models through multi-step pruning policy via reinforcement learning. *Information Sciences* 686 (2025), 121361.
- [17] Ahmed Hendawy, Jan Peters, and Carlo D’Eramo. 2024. Multi-Task Reinforcement Learning with Mixture of Orthogonal Experts. In *The Twelfth International Conference on Learning Representations*. <https://openreview.net/forum?id=aZH1dM3GOX>
- [18] Nuowen Kan, Yuankun Jiang, Chenglin Li, Wenrui Dai, Junni Zou, and Hongkai Xiong. 2022. Improving generalization for neural adaptive video streaming via meta reinforcement learning. In *Proceedings of the 30th ACM International Conference on Multimedia*. 3006–3016.
- [19] Nuowen Kan, Chenglin Li, Caiyi Yang, Wenrui Dai, Junni Zou, and Hongkai Xiong. 2021. Uncertainty-aware robust adaptive video streaming with bayesian neural network and model predictive control. In *Proceedings of the 31st ACM Workshop on Network and Operating Systems Support for Digital Audio and Video (Istanbul, Turkey) (NOSSDAV ’21)*. Association for Computing Machinery, New York, NY, USA, 17–24. <https://doi.org/10.1145/3458306.3458872>
- [20] Takuto Kimura, Tatsuaki Kimura, and Kazuhisa Yamagishi. 2021. Context-aware adaptive bitrate streaming system. In *ICC 2021-IEEE International Conference on Communications*. IEEE, 1–7.
- [21] Dongkeun Lee, Minwoo Joo, and Wonjun Lee. 2022. Qrator: An Interest-Aware Approach to ABR Streaming Based on User Engagement. *IEEE Systems Journal* 16, 4 (2022), 6581–6589.
- [22] Hojoon Lee, Hyeonseong Cho, Hyunseung Kim, Donghu Kim, Dugki Min, Jaegul Choo, and Clare Lyle. 2024. Slow and Steady Wins the Race: Maintaining Plasticity with Hare and Tortoise Networks. In *Proceedings of the 41st International Conference on Machine Learning (Proceedings of Machine Learning Research, Vol. 235)*. Ruslan Salakhutdinov, Zico Kolter, Katherine Heller, Adrian Weller, Nuria Oliver, Jonathan Scarlett, and Felix Berkenkamp (Eds.). PMLR, 26416–26438. <https://proceedings.mlr.press/v235/lee24d.html>
- [23] Mike Lewis, Shruti Bhosale, Tim Dettmers, Naman Goyal, and Luke Zettlemoyer. 2021. Base layers: Simplifying training of large, sparse models. In *International Conference on Machine Learning*. PMLR, 6265–6274.
- [24] Hongbo Li and Lingjie Duan. 2024. Theory of Mixture-of-Experts for Mobile Edge Computing. *CoRR abs/2412.15690* (2024). <http://dblp.uni-trier.de/db/journals/corr/corr2412.html#abs-2412-15690>
- [25] Hongbo Li, Sen Lin, Lingjie Duan, Yingbin Liang, and Ness Shroff. 2025. Theory on Mixture-of-Experts in Continual Learning. In *The Thirteenth International Conference on Learning Representations*. <https://openreview.net/forum?id=7XgKAabsPp>
- [26] Jing Li, Zhijie Sun, Xuan He, Li Zeng, Yi Lin, Entong Li, Binfan Zheng, Rongqian Zhao, and Xin Chen. 2024. LocMoE: A Low-overhead MoE for Large Language Model Training. In *IJCAI*. ijcai.org, 6377–6387. <http://dblp.uni-trier.de/db/conf/ijcai/ijcai2024.html#LiSZLLZZC24>
- [27] Weihe Li, Jiawei Huang, Shiqi Wang, Chuliang Wu, Sen Liu, and Jianxin Wang. 2023. An Apprenticeship Learning Approach for Adaptive Video Streaming Based on Chunk Quality and User Preference. *IEEE Transactions on Multimedia* 25 (2023), 2488–2502. <https://doi.org/10.1109/TMM.2022.3147667>
- [28] Wenzhong Li, Xiang Li, Yeting Xu, Yi Yang, and Sanglu Lu. 2023. Metaabr: A meta-learning approach on adaptive bitrate selection for video streaming. *IEEE Transactions on Mobile Computing* 23, 3 (2023), 2422–2437.
- [29] Bin Lin, Zhenyu Tang, Yang Ye, Jiayi Cui, Bin Zhu, Peng Jin, Junwu Zhang, Muan Ning, and Li Yuan. 2024. MoE-LLaVA: Mixture of Experts for Large Vision-Language Models. *CoRR abs/2401.15947* (2024). <http://dblp.uni-trier.de/db/journals/corr/corr2401.html#abs-2401-15947>
- [30] Na Lin, Yamei Wang, Enchao Zhang, Shaohua Wan, Ahmed Al-Dubai, and Liang Zhao. 2024. User Preferences-Based Proactive Content Caching with Characteristics Differentiation in HetNets. *IEEE Transactions on Sustainable Computing* (2024), 1–12. <https://doi.org/10.1109/TSUSC.2024.3441606>
- [31] Clare Lyle, Zeyu Zheng, Evgenii Nikishin, Bernardo Ávila Pires, Razvan Pascanu, and Will Dabney. 2023. Understanding Plasticity in Neural Networks. In *ICML (Proceedings of Machine Learning Research, Vol. 202)*. PMLR, 23190–23211. <http://dblp.uni-trier.de/db/conf/icml/icml2023.html#LyleZNPDP23>
- [32] Hongzi Mao, Ravi Netravali, and Mohammad Alizadeh. 2017. Neural adaptive video streaming with pensieve. In *Proceedings of the conference of the ACM special interest group on data communication*. 197–210.
- [33] Michal Nauman, Mateusz Ostaszewski, Krzysztof Jankowski, Piotr Miloś, and Marek Cygan. 2025. Bigger, regularized, optimistic: scaling for compute and sample efficient continuous control. *Advances in Neural Information Processing Systems* 37 (2025), 113038–113071.
- [34] Evgenii Nikishin, Max Schwarzer, Pierluca D’Oro, Pierre-Luc Bacon, and Aaron Courville. 2022. The primacy bias in deep reinforcement learning. In *International conference on machine learning*. PMLR, 16828–16847.
- [35] Johan Samir Obando Ceron, Aaron Courville, and Pablo Samuel Castro. 2024. In value-based deep reinforcement learning, a pruned network is a good network. In *Proceedings of the 41st International Conference on Machine Learning (Proceedings of Machine Learning Research, Vol. 235)*. Ruslan Salakhutdinov, Zico Kolter, Katherine Heller, Adrian Weller, Nuria Oliver, Jonathan Scarlett, and Felix Berkenkamp (Eds.). PMLR, 38495–38519.
- [36] Matt Puderbaugh and Prabhu D Emmady. 2023. Neuroplasticity. In *StatPearls [Internet]*. StatPearls Publishing.
- [37] Joan Puigcerver, Carlos Riquelme Ruiz, Basil Mustafa, and Neil Houlsby. 2024. From Sparse to Soft Mixtures of Experts. In *The Twelfth International Conference on Learning Representations*. <https://openreview.net/forum?id=jxpsAj7lTE>
- [38] Stephen Roller, Sainbayar Sukhbaatar, Arthur Szlam, and Jason E Weston. 2021. Hash Layers For Large Sparse Models. In *Advances in Neural Information Processing Systems*, A. Beygelzimer, Y. Dauphin, P. Liang, and J. Wortman Vaughan (Eds.). <https://openreview.net/forum?id=lmGDDWb1ULW>
- [39] Olivier Roy and Martin Vetterli. 2007. The effective rank: A measure of effective dimensionality. In *2007 15th European Signal Processing Conference*. 606–610.
- [40] John Schulman, Filip Wolski, Prafulla Dhariwal, Alec Radford, and Oleg Klimov. 2017. Proximal policy optimization algorithms. *arXiv preprint arXiv:1707.06347* (2017).
- [41] Max Schwarzer, Johan Samir Obando Ceron, Aaron Courville, Marc G Bellemare, Rishabh Agarwal, and Pablo Samuel Castro. 2023. Bigger, better, faster: Human-level atari with human-level efficiency. In *International Conference on Machine Learning*. PMLR, 30365–30380.
- [42] Noam Shazeer, \*Azalia Mirhoseini, \*Krzysztof Maziarz, Andy Davis, Quoc Le, Geoffrey Hinton, and Jeff Dean. 2017. Outrageously Large Neural Networks: The Sparsely-Gated Mixture-of-Experts Layer. In *International Conference on Learning Representations*. <https://openreview.net/forum?id=B1ckMDqIqg>

- [43] Baekrok Shin, Junsoo Oh, Hanseul Cho, and Chulhee Yun. 2024. DASH: Warm-Starting Neural Network Training Without Loss of Plasticity Under Stationarity. In *2nd Workshop on Advancing Neural Network Training: Computational Efficiency, Scalability, and Resource Optimization (WANT@ICML 2024)*. <https://openreview.net/forum?id=GR5LXaglgG>
- [44] Ghada Sokar, Rishabh Agarwal, Pablo Samuel Castro, and Utku Evci. 2023. The dormant neuron phenomenon in deep reinforcement learning. In *International Conference on Machine Learning*. PMLR, 32145–32168.
- [45] Lingfeng Sun, Haichao Zhang, Wei Xu, and Masayoshi Tomizuka. 2022. Paco: Parameter-compositional multi-task reinforcement learning. *Advances in Neural Information Processing Systems* 35 (2022), 21495–21507.
- [46] Kexin Tang, Nuowen Kan, Yuankun Jiang, Chenglin Li, Wenrui Dai, Junni Zou, and Hongkai Xiong. 2023. Successor Feature-Based Transfer Reinforcement Learning for Video Rate Adaptation With Heterogeneous QoE Preferences. *IEEE Transactions on Multimedia* 26 (2023), 5340–5357.
- [47] Kexin Tang, Nuowen Kan, Yuankun Jiang, Chenglin Li, Wenrui Dai, Junni Zou, and Hongkai Xiong. 2024. Successor Feature-Based Transfer Reinforcement Learning for Video Rate Adaptation With Heterogeneous QoE Preferences. *IEEE Transactions on Multimedia* 26 (2024), 5340–5357. <https://doi.org/10.1109/TMM.2023.3331487>
- [48] Mathieu Blondel Tianlin Liu, Joan Puigcerver. 2023. Sparsity-constrained optimal transport. In *Proceedings of the Eleventh International Conference on Learning Representations (ICLR)*. <https://openreview.net/forum?id=yHY9NbQJ5BP>
- [49] Shuoyao Wang, Jiawei Lin, and Yu Dai. 2024. MMVS: Enabling robust adaptive video streaming for wildly fluctuating and heterogeneous networks. *IEEE Transactions on Multimedia* (2024).
- [50] Timon Willi, Johan Samir Obando-Ceron, Jakob Nicolaus Foerster, Gintare Karolina Dziugaite, and Pablo Samuel Castro. 2024. Mixture of Experts in a Mixture of RL settings. *RLJ* 3 (2024), 1072–1105. <http://dblp.uni-trier.de/db/journals/rlj/rlj3.html#WilliOFDC24>
- [51] Timon Willi, Johan Samir Obando-Ceron, Jakob Nicolaus Foerster, Gintare Karolina Dziugaite, and Pablo Samuel Castro. 2024. Mixture of Experts in a Mixture of RL settings. *RLJ* 3 (2024), 1072–1105. <http://dblp.uni-trier.de/db/journals/rlj/rlj3.html#WilliOFDC24>
- [52] Fuzhao Xue, Zian Zheng, Yao Fu, Jinjie Ni, Zangwei Zheng, Wangchunshu Zhou, and Yang You. 2024. OpenMoE: an early effort on open mixture-of-experts language models. In *Proceedings of the 41st International Conference on Machine Learning (Vienna, Austria) (ICML'24)*. JMLR.org, Article 2293, 31 pages.
- [53] Yuzhe Yang, Guo Zhang, Zhi Xu, and Dina Katabi. 2020. Harnessing Structures for Value-Based Planning and Reinforcement Learning. In *International Conference on Learning Representations*. <https://openreview.net/forum?id=rklHqRVKvH>
- [54] Lei Zhang, Guanyu Gao, and Huaizheng Zhang. 2022. Towards data-efficient continuous learning for edge video analytics via smart caching. In *Proceedings of the 20th ACM Conference on Embedded Networked Sensor Systems*. 1136–1140.
- [55] Xu Zhang, Yiyang Ou, Siddhartha Sen, and Junchen Jiang. 2021. {SENSEI}: Aligning video streaming quality with dynamic user sensitivity. In *18th USENIX Symposium on Networked Systems Design and Implementation (NSDI 21)*. 303–320.
- [56] Xu Zhang, Paul Schmitt, Marshini Chetty, Nick Feamster, and Junchen Jiang. 2022. Enabling personalized video quality optimization with VidHoc. *arXiv preprint arXiv:2211.15959* (2022).
- [57] Junfang Zheng, Junling Shi, Qiang He, Enchao Zhang, Ammar Hawbani, and Liang Zhao. 2023. An Influence Maximization-Based Hybrid Advertising Dissemination for Internet of Vehicles. *IEEE Networking Letters* 5, 4 (2023), 218–222. <https://doi.org/10.1109/LNET.2023.3296081>
- [58] Yanqi Zhou, Tao Lei, Hanxiao Liu, Nan Du, Yanping Huang, Vincent Zhao, Andrew M Dai, Quoc V Le, James Laudon, et al. 2022. Mixture-of-experts with expert choice routing. *Advances in Neural Information Processing Systems* 35 (2022), 7103–7114.
- [59] Xutong Zuo, Jiayu Yang, Mowei Wang, and Yong Cui. 2022. Adaptive Bitrate with User-level QoE Preference for Video Streaming. In *IEEE INFOCOM 2022 - IEEE Conference on Computer Communications*. 1279–1288. <https://doi.org/10.1109/INFOCOM48880.2022.9796953>

## A Proof of Gradient Co-coercivity Lemma Proof.

**Lemma 4.1: (Gradient Co-coercivity Lemma.)** Let  $L_t : \mathbb{R}^d \rightarrow \mathbb{R}$  be an  $L$ -smooth function; that is, for all  $\mathbf{w}, \mathbf{w}' \in \mathbb{R}^d$ ,

$$\|\nabla L_t(\mathbf{w}) - \nabla L_t(\mathbf{w}')\| \leq L\|\mathbf{w} - \mathbf{w}'\|.$$

Then, for any  $\mathbf{w}_i^t, \mathbf{w}_i^* \in \mathbb{R}^d$ , we have

$$\begin{aligned} \|\nabla L_t(\mathbf{w}_i^t) - \nabla L_t(\mathbf{w}_i^*)\|^2 \\ \leq L(\nabla L_t(\mathbf{w}_i^t) - \nabla L_t(\mathbf{w}_i^*))^T(\mathbf{w}_i^t - \mathbf{w}_i^*). \end{aligned} \quad (16)$$

PROOF. Since  $L_t$  is  $L$ -smooth, we immediately have

$$\|\nabla L_t(\mathbf{w}_i^t) - \nabla L_t(\mathbf{w}_i^*)\| \leq L\|\mathbf{w}_i^t - \mathbf{w}_i^*\|.$$

Multiplying both sides by  $\|\mathbf{w}_i^t - \mathbf{w}_i^*\|$  yields

$$\begin{aligned} 0 &\leq L\|\mathbf{w}_i^t - \mathbf{w}_i^*\|^2 - \|\nabla L_t(\mathbf{w}_i^t) - \nabla L_t(\mathbf{w}_i^*)\| \|\mathbf{w}_i^t - \mathbf{w}_i^*\| \\ &\leq L\|\mathbf{w}_i^t - \mathbf{w}_i^*\|^2 - (\nabla L_t(\mathbf{w}_i^t) - \nabla L_t(\mathbf{w}_i^*))^T(\mathbf{w}_i^t - \mathbf{w}_i^*) \\ &\leq (L\mathbf{w}_i^t - \nabla L_t(\mathbf{w}_i^t) - L\mathbf{w}_i^* + \nabla L_t(\mathbf{w}_i^*))(\mathbf{w}_i^t - \mathbf{w}_i^*). \end{aligned}$$

Next, define the auxiliary function

$$g(\mathbf{w}) := \frac{1}{2}L\mathbf{w}^T\mathbf{w} - L_t(\mathbf{w}),$$

so that

$$\nabla g(\mathbf{w}) = L\mathbf{w} - \nabla L_t(\mathbf{w}).$$

Because  $L_t$  is  $L$ -smooth, one may verify that  $g(\mathbf{w})$  is convex. Hence, for any  $\mathbf{w}_i^t$  and  $\mathbf{w}_i^*$  we have

$$g(\mathbf{w}_i^t) \geq g(\mathbf{w}_i^*) + \nabla g(\mathbf{w}_i^*)^T(\mathbf{w}_i^t - \mathbf{w}_i^*),$$

that is,

$$\begin{aligned} \frac{L}{2}\|\mathbf{w}_i^t\|^2 - L_t(\mathbf{w}_i^t) \\ \geq \frac{L}{2}\|\mathbf{w}_i^*\|^2 - L_t(\mathbf{w}_i^*) + (L\mathbf{w}_i^* - \nabla L_t(\mathbf{w}_i^*))^T(\mathbf{w}_i^t - \mathbf{w}_i^*). \end{aligned} \quad (17)$$

Rearranging (17) gives

$$\frac{L}{2}\|\mathbf{w}_i^t - \mathbf{w}_i^*\|^2 \geq L_t(\mathbf{w}_i^t) - L_t(\mathbf{w}_i^*) - \nabla L_t(\mathbf{w}_i^*)^T(\mathbf{w}_i^t - \mathbf{w}_i^*). \quad (18)$$

Now, introduce the point

$$z = \mathbf{w}_i^* + \frac{1}{L}(\nabla L_t(\mathbf{w}_i^t) - \nabla L_t(\mathbf{w}_i^*)).$$

Using a standard descent argument and the smoothness of  $L_t$ , one can write

$$\begin{aligned} L_t(\mathbf{w}_i^*) - L_t(\mathbf{w}_i^t) &= [L_t(\mathbf{w}_i^*) - L_t(z)] + [L_t(z) - L_t(\mathbf{w}_i^t)] \\ &\geq -\nabla L_t(\mathbf{w}_i^*)^T(z - \mathbf{w}_i^*) - \frac{L}{2}\|z - \mathbf{w}_i^*\|^2 \\ &\quad + \nabla L_t(\mathbf{w}_i^t)^T(z - \mathbf{w}_i^t). \end{aligned} \quad (19)$$

Observing that

$$z - \mathbf{w}_i^* = \frac{1}{L}(\nabla L_t(\mathbf{w}_i^t) - \nabla L_t(\mathbf{w}_i^*))$$

and

$$z - \mathbf{w}_i^t = (\mathbf{w}_i^* - \mathbf{w}_i^t) + \frac{1}{L}(\nabla L_t(\mathbf{w}_i^t) - \nabla L_t(\mathbf{w}_i^*)),$$

one obtains after elementary algebra that (19) can be rearranged to

$$L_t(\mathbf{w}_i^*) - L_t(\mathbf{w}_i^t) \geq \nabla L_t(\mathbf{w}_i^t)^T(\mathbf{w}_i^* - \mathbf{w}_i^t) + \frac{1}{2L}\|\nabla L_t(\mathbf{w}_i^t) - \nabla L_t(\mathbf{w}_i^*)\|^2.$$

In other words,

$$L_t(\mathbf{w}_i^*) \geq L_t(\mathbf{w}_i^t) + \nabla L_t(\mathbf{w}_i^t)^T(\mathbf{w}_i^* - \mathbf{w}_i^t) + \frac{1}{2L}\|\nabla L_t(\mathbf{w}_i^t) - \nabla L_t(\mathbf{w}_i^*)\|^2,$$

$$L_t(\mathbf{w}_i^t) \geq L_t(\mathbf{w}_i^*) + \nabla L_t(\mathbf{w}_i^*)^T(\mathbf{w}_i^t - \mathbf{w}_i^*) + \frac{1}{2L}\|\nabla L_t(\mathbf{w}_i^t) - \nabla L_t(\mathbf{w}_i^*)\|^2.$$

Adding the two relations (or, equivalently, combining them appropriately) leads to

$$L(\nabla L_t(\mathbf{w}_i^t) - \nabla L_t(\mathbf{w}_i^*))^T(\mathbf{w}_i^t - \mathbf{w}_i^*) \geq \|\nabla L_t(\mathbf{w}_i^t) - \nabla L_t(\mathbf{w}_i^*)\|^2.$$

This completes the proof of (16).  $\square$

## B Gradient Strong Convexity Lemma Proof.

**Lemma 4.2: (Gradient Strong Convexity Lemma.)** Let  $L_t : \mathbb{R}^d \rightarrow \mathbb{R}$  be a  $\mu$ -strongly convex function; that is, for all  $\mathbf{w}, \mathbf{w}' \in \mathbb{R}^d$ ,

$$L_t(\mathbf{w}') \geq L_t(\mathbf{w}) + \nabla L_t(\mathbf{w})^T(\mathbf{w}' - \mathbf{w}) + \frac{\mu}{2}\|\mathbf{w}' - \mathbf{w}\|^2.$$

Then, for any  $\mathbf{w}_i^t, \mathbf{w}_i^* \in \mathbb{R}^d$ , it holds that

$$(\nabla L_t(\mathbf{w}_i^t) - \nabla L_t(\mathbf{w}_i^*))^T(\mathbf{w}_i^t - \mathbf{w}_i^*) \geq \mu\|\mathbf{w}_i^t - \mathbf{w}_i^*\|^2. \quad (20)$$

PROOF. Since  $L_t$  is  $\mu$ -strongly convex, for any  $\mathbf{w}, \mathbf{w}' \in \mathbb{R}^d$  we have

$$L_t(\mathbf{w}') \geq L_t(\mathbf{w}) + \nabla L_t(\mathbf{w})^T(\mathbf{w}' - \mathbf{w}) + \frac{\mu}{2}\|\mathbf{w}' - \mathbf{w}\|^2, \quad (21)$$

$$L_t(\mathbf{w}) \geq L_t(\mathbf{w}') + \nabla L_t(\mathbf{w}')^T(\mathbf{w} - \mathbf{w}') + \frac{\mu}{2}\|\mathbf{w} - \mathbf{w}'\|^2. \quad (22)$$

Adding (21) and (22) yields

$$0 \geq \nabla L_t(\mathbf{w})^T(\mathbf{w}' - \mathbf{w}) + \nabla L_t(\mathbf{w}')^T(\mathbf{w} - \mathbf{w}') + \mu\|\mathbf{w}' - \mathbf{w}\|^2.$$

Noting that

$$\nabla L_t(\mathbf{w}')^T(\mathbf{w} - \mathbf{w}') = -\nabla L_t(\mathbf{w}')^T(\mathbf{w}' - \mathbf{w}),$$

we deduce

$$(\nabla L_t(\mathbf{w}) - \nabla L_t(\mathbf{w}'))^T(\mathbf{w}' - \mathbf{w}) \geq \mu\|\mathbf{w}' - \mathbf{w}\|^2.$$

Setting  $\mathbf{w} = \mathbf{w}_i^t$  and  $\mathbf{w}' = \mathbf{w}_i^*$  completes the proof.  $\square$

## C Expert Tracking Theory Proof

**Lemma 4.3: (Parameterized Norm Inequality.)** Let  $a, b$  be elements of a real inner product space and  $\alpha > 0$ . Then:

$$\|a + b\|^2 \leq (1 + \alpha)\|a\|^2 + (1 + \alpha^{-1})\|b\|^2 \quad (23)$$

PROOF. First expand the left-hand side:

$$\|a + b\|^2 = \|a\|^2 + 2\langle a, b \rangle + \|b\|^2 \quad (24)$$

The right-hand side expands to:

$$(1 + \alpha)\|a\|^2 + (1 + \alpha^{-1})\|b\|^2 = \|a\|^2 + \alpha\|a\|^2 + \|b\|^2 + \alpha^{-1}\|b\|^2.$$

Comparing both sides, it suffices to show:

$$2\langle a, b \rangle \leq \alpha\|a\|^2 + \alpha^{-1}\|b\|^2 \quad (25)$$

This follows from Young's inequality  $2xy \leq \alpha x^2 + \alpha^{-1}y^2$  applied to  $x = \|a\|$  and  $y = \|b\|$ , combined with Cauchy-Schwarz inequality  $\langle a, b \rangle \leq \|a\|\|b\|$ .  $\square$

**Theorem 4.3: (Expert Tracking Theory.)** Under Assumptions (A1)–(A3) and with the update rule

$$\mathbf{w}_i^{t+1} = \mathbf{w}_i^t - \eta \nabla L_t(\mathbf{w}_i^t) + \eta \gamma \epsilon_i^t, \quad \epsilon_i^t \sim \mathcal{N}(0, I_d), \quad (26)$$

there exists a constant  $C > 0$  (depending only on  $L$  and  $\mu$ ) such that the average squared error satisfies

$$\frac{1}{T} \sum_{t=1}^T \mathbb{E} \|e_t\|^2 \leq C \left( \eta \gamma^2 d + \frac{P_T^2}{T\eta} \right), \quad (27)$$

where the error is defined as  $e_t = \mathbf{w}_i^t - \mathbf{w}_i^*$  and the path length of the optimal parameters is

$$P_T = \sum_{t=1}^{T-1} \|\mathbf{w}_{t+1}^* - \mathbf{w}_t^*\|.$$

PROOF. Define the drift of the optimal parameter as

$$\Delta_t := \mathbf{w}_{t+1}^* - \mathbf{w}_t^*. \quad (28)$$

Then the error update is

$$\begin{aligned} e_{t+1} &= \mathbf{w}_i^{t+1} - \mathbf{w}_{t+1}^* \\ &= \mathbf{w}_i^t - \eta \nabla L_t(\mathbf{w}_i^t) + \eta \gamma \epsilon_i^t - \mathbf{w}_{t+1}^* \\ &= \underbrace{\left[ \mathbf{w}_i^t - \mathbf{w}_t^* - \eta \left( \nabla L_t(\mathbf{w}_i^t) - \nabla L_t(\mathbf{w}_t^*) \right) \right]}_{=: A_t} - \underbrace{\Delta_t}_{=: E_t} + \underbrace{\eta \gamma \epsilon_i^t}_{=: \text{Noise Term}} \\ &= \underbrace{(e_t - \eta \left( \nabla L_t(\mathbf{w}_i^t) - \nabla L_t(\mathbf{w}_t^*) \right))}_{\text{Contraction Term } A_t} - \underbrace{\Delta_t}_{\text{Drift Term}} + \underbrace{\eta \gamma \epsilon_i^t}_{\text{Noise Term}}. \end{aligned} \quad (29)$$

Thus,

$$e_{t+1} = A_t - \Delta_t + E_t. \quad (29)$$

**Step 1: Contraction Property of  $A_t$ .** We now show that under the conditions of  $\mu$ -strong convexity and  $L$ -smoothness (with assumption  $\eta \leq 1/L$ ), it holds that

$$\|A_t\|^2 \leq (1 - \mu\eta) \|e_t\|^2. \quad (30)$$

Indeed, by definition,

$$A_t = e_t - \eta \left( \nabla L_t(\mathbf{w}_i^t) - \nabla L_t(\mathbf{w}_t^*) \right).$$

Expanding the square norm, we obtain:

$$\begin{aligned} \|A_t\|^2 &= \|e_t\|^2 - 2\eta \langle e_t, \nabla L_t(\mathbf{w}_i^t) - \nabla L_t(\mathbf{w}_t^*) \rangle \\ &\quad + \eta^2 \|\nabla L_t(\mathbf{w}_i^t) - \nabla L_t(\mathbf{w}_t^*)\|^2. \end{aligned} \quad (31)$$

Since  $L_t$  is  $\mu$ -strongly convex, it satisfies (Lemma 4.2)

$$\langle e_t, \nabla L_t(\mathbf{w}_i^t) - \nabla L_t(\mathbf{w}_t^*) \rangle \geq \mu \|e_t\|^2.$$

Moreover, by  $L$ -smoothness (Lemma 4.1),

$$\|\nabla L_t(\mathbf{w}_i^t) - \nabla L_t(\mathbf{w}_t^*)\|^2 \leq L \langle e_t, \nabla L_t(\mathbf{w}_i^t) - \nabla L_t(\mathbf{w}_t^*) \rangle.$$

Hence,

$$\eta^2 \|\nabla L_t(\mathbf{w}_i^t) - \nabla L_t(\mathbf{w}_t^*)\|^2 \leq \eta^2 L \langle e_t, \nabla L_t(\mathbf{w}_i^t) - \nabla L_t(\mathbf{w}_t^*) \rangle.$$

Substituting these bounds back, we have

$$\begin{aligned} \|A_t\|^2 &\leq \|e_t\|^2 - 2\eta \langle e_t, \nabla L_t(\mathbf{w}_i^t) - \nabla L_t(\mathbf{w}_t^*) \rangle \\ &\quad + \eta^2 L \langle e_t, \nabla L_t(\mathbf{w}_i^t) - \nabla L_t(\mathbf{w}_t^*) \rangle. \end{aligned}$$

That is,

$$\|A_t\|^2 \leq \|e_t\|^2 - \eta(2 - \eta L) \langle e_t, \nabla L_t(\mathbf{w}_i^t) - \nabla L_t(\mathbf{w}_t^*) \rangle.$$

Using the strong convexity bound  $\langle e_t, \nabla L_t(\mathbf{w}_i^t) - \nabla L_t(\mathbf{w}_t^*) \rangle \geq \mu \|e_t\|^2$  leads to

$$\|A_t\|^2 \leq \left[ 1 - \eta\mu(2 - \eta L) \right] \|e_t\|^2.$$

Since  $\eta \leq \frac{1}{L}$  implies  $2 - \eta L \geq 1$ , it follows that

$$\|A_t\|^2 \leq (1 - \eta\mu) \|e_t\|^2.$$

**Step 2: Recursive Inequality with Noise-Drift Coupling.**

Expanding  $\|e_{t+1}\|^2$ :

$$\|e_{t+1}\|^2 \leq \|A_t - \Delta_t\|^2 + 2\eta\gamma \langle A_t - \Delta_t, \epsilon_i^t \rangle + \eta^2 \gamma^2 \|\epsilon_i^t\|^2 \quad (32)$$

Taking expectations (note  $\mathbb{E}[\epsilon_i^t] = 0$ ):

$$\mathbb{E} \|e_{t+1}\|^2 \leq \mathbb{E} \|A_t - \Delta_t\|^2 + \eta^2 \gamma^2 d. \quad (33)$$

Applying Lemma 4.3:  $\|a + b\|^2 \leq (1 + \alpha)\|a\|^2 + (1 + \alpha^{-1})\|b\|^2$  (for  $\alpha > 0$ ) to  $\mathbb{E} \|A_t - \Delta_t\|^2$ :

$$\mathbb{E} \|e_{t+1}\|^2 \leq (1 + \alpha)(1 - \mu\eta) \mathbb{E} \|e_t\|^2 + (1 + \alpha^{-1}) \|\Delta_t\|^2 + \eta^2 \gamma^2 d.$$

Set  $\alpha = \mu\eta/2$  ensuring  $(1 + \alpha)(1 - \mu\eta) \leq 1 - \mu\eta/2$ . This yield:

$$\mathbb{E} \|e_{t+1}\|^2 \leq \left( 1 - \frac{\mu\eta}{2} \right) \mathbb{E} \|e_t\|^2 + \frac{2}{\mu\eta} \|\Delta_t\|^2 + \eta^2 \gamma^2 d. \quad (34)$$

**Step 3: Telescoping Sum and Final Bound.**

Unrolling the recursion over  $t$ :

$$\begin{aligned} \mathbb{E} \|e_t\|^2 &\leq \left( 1 - \frac{\mu\eta}{2} \right)^t \mathbb{E} \|e_0\|^2 + \frac{2}{\mu\eta} \sum_{k=0}^{t-1} \left( 1 - \frac{\mu\eta}{2} \right)^{t-1-k} \|\Delta_k\|^2 + \\ &\quad \eta^2 \gamma^2 d \sum_{k=0}^{t-1} \left( 1 - \frac{\mu\eta}{2} \right)^k \end{aligned} \quad (35)$$

Summing and averaging the Error from  $t = 1$  to  $T$ . The initial error term can be expressed as:

$$\frac{1}{T} \sum_{t=1}^T \left( 1 - \frac{\mu\eta}{2} \right)^t \mathbb{E} \|e_0\|^2 \leq \frac{1}{T} \cdot \frac{2}{\mu\eta} \mathbb{E} \|e_0\|^2. \quad (36)$$

For the drift term, interchange summation order and utilizing the geometric series formula:

$$\frac{1}{T} \sum_{t=1}^T \frac{2}{\mu\eta} \sum_{k=0}^{t-1} \left( 1 - \frac{\mu\eta}{2} \right)^{t-1-k} \|\Delta_k\|^2 \leq \frac{1}{T} \cdot \frac{4}{\mu^2 \eta^2} \sum_{k=0}^{T-1} \|\Delta_k\|^2 \quad (37)$$

The noise contribution at each time step follows a geometric series:

$$\frac{1}{T} \sum_{t=1}^T \eta^2 \gamma^2 d \sum_{k=0}^{t-1} \left( 1 - \frac{\mu\eta}{2} \right)^k \leq \frac{1}{T} \cdot \frac{2\eta\gamma^2 d T}{\mu}. \quad (38)$$

For large  $T$  the initial error term is negligible, and after a refined constant adjustment, we arrive at

$$\frac{1}{T} \sum_{t=1}^T \mathbb{E} \|e_t\|^2 \leq \frac{4P_T^2}{\mu^2 \eta^2 T} + \frac{2\eta\gamma^2 d}{\mu} \quad (39)$$

$$\leq C \left( \eta\gamma^2 d + \frac{P_T^2}{T\eta} \right) \quad (40)$$

Here, we absorb the coefficients of the higher-order terms into a constant  $C$  and implicitly impose the step-size constraint  $\frac{4}{\mu^2\eta^2} \leq \frac{C}{\eta}$ . In practical algorithms, the step size is usually small (e.g.,  $\eta \leq \frac{1}{L}$ ); thus, this constraint naturally holds in most scenarios. In doing so, we sacrifice some precision but are better able to capture the dynamic balance between the two factors.  $\square$

## D Implementation Detail

All experiments were performed on a system equipped with an Intel(R) Core(TM) i5-10400 CPU @ 2.90GHz, without GPU acceleration. The Adaptive Video System adopts the parameter settings from Pensieve [32]. PPO hyperparameters are detailed in Table 1. For each training run, the agent is trained for approximately two hours, with a total of 2 million timesteps and 1000 iterations.

**Table 1: Potential Hyperparameters Configurations For PPO.**

Hyperparameter	Value
Number of Environments	1
Learning Rate	1e-4
batch size	2000
Minibatch Size	62
Number of Iteration	1000
Steps	2000
Total Timesteps	2e6
Update Epochs	5
GAE- $\gamma$	0.99
GAE- $\lambda$	0.95
Clip $\epsilon$	0.2
Entropy Coefficient	0
Value Function Coefficient	5
Max Gradient Norm	False
Activation	ReLU
Environment	{D, L, N}
Anneal learning rate	False
# Experts	3
Expert Hidden Size	18
MoE	{MoE, SMoE, PA-MoE}
Router	{Top-K-Router, Softmax-Router}
Number of Selected Experts	1
Actor MoE	True
Critic MoE	True

## E Expert Contributions to Mitigating Plasticity Loss in PA-MoE

In this subsection, we use the Dormant Neuron Ratio as a quantitative metric to visualize and analyze the extent of plasticity loss within the neural network. This metric allows us to measure the number of inactive or underutilized neurons during the training process, which is often associated with decreased expressiveness and adaptability in deep models, particularly in continual or multitask learning scenarios. Monitoring neuron dormancy is crucial for understanding how effectively a model utilizes its capacity, especially in complex modular architectures like PA-MoE.

To formalize this, we introduce the following definition:

**Definition E.1 (Dormant Neuron).** Consider a neural network layer  $l$  consisting of  $H_l$  neurons. We define the dormancy index  $s_{l,i}$  of the  $i$ -th neuron in layer  $l$  as:

$$s_{l,i} = \frac{\mathbb{E}_{\mathbf{x} \in D} |h_{l,i}(\mathbf{x})|}{\frac{1}{H_l} \sum_{j \in h} \mathbb{E}_{\mathbf{x} \in D} |h_{l,j}(\mathbf{x})|}, \quad (41)$$

where  $h_{l,i}(\mathbf{x})$  denotes the activation of neuron  $(l, i)$  given input  $\mathbf{x}$ , and  $\mathbb{E}_{\mathbf{x} \in D}$  denotes the expectation over input samples drawn from the data distribution  $D$ .

A neuron is considered dormant if its dormancy index  $s_{l,i}$  falls below a certain threshold, indicating that its average activation is significantly lower than the average activation across the layer. A high ratio of dormant neurons suggests a loss of plasticity, where large portions of the network are no longer contributing meaningfully to the model’s output.

The experimental results are visualized in Figure 11, where we plot the Layer Dormant (LD) ratios for each expert in the PA-MoE framework. These visualizations cover both the policy and value networks and provide an insightful cross-layer analysis.

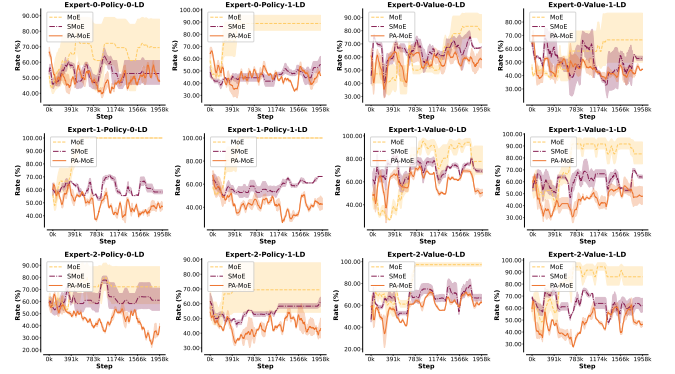


**Figure 11: Visualization results of the dormant neuron (Layer Dormant, LD) ratios across different layers of the policy and value networks for various experts.**

As shown in the Figure 11, PA-MoE consistently maintains a lower proportion of dormant neurons across different experts and layers compared to baseline models. This suggests that PA-MoE’s architectural design—particularly its noise-injection mechanism and adaptive routing—helps in better utilization of network capacity, encouraging more balanced activation across neurons and reducing the risk of premature convergence or feature stagnation.

## F Layer-wise Analysis of Expert Rank in PA-MoE

In order to gain a deeper understanding of plasticity loss and its impact on the internal representations of neural networks, we complement our analysis of dormant neurons with a study of the feature rank of hidden layer activations. While the Dormant Neuron Ratio captures how many neurons become underutilized or inactive during training, it does not fully reveal whether the active neurons

are producing diverse or redundant outputs. Thus, we introduce the Rank of Batch Hidden Layer Output as an additional diagnostic tool to evaluate the expressive capacity and dimensional richness of hidden representations.

This metric allows us to investigate whether PA-MoE not only keeps neurons active, but also ensures that their activations span a high-dimensional space—an essential characteristic for maintaining plasticity and avoiding feature collapse. A model that suffers from plasticity loss often shows not just fewer active neurons, but also lower-rank activation patterns, indicating that different inputs are being mapped to similar internal states. Conversely, a higher feature rank suggests that the model retains the ability to differentiate among inputs and adapt its representations accordingly.

In the following, we formally define the rank metric and present our empirical observations through visualizations of rank values across layers and experts under different MoE configurations.

**Definition F.1 (Rank of Batch Hidden Layer Output).** Let a hidden layer consist of  $H$  neurons. For a batch of inputs of size  $B$ , the layer's output forms a matrix  $M \in \mathbb{R}^{B \times H}$ , where each row represents the activation vector of a single sample. We define the rank of  $M$  as the number of linearly independent rows (or columns), which is equivalent to the number of nonzero singular values obtained via singular value decomposition (SVD). Formally, if  $\{\sigma_i\}$  are the singular values of  $M$ , then

$$\text{rank}(M) = \#\{i \mid \sigma_i > 0\}. \quad (42)$$

This metric quantifies the diversity and effective dimensionality of the hidden layer's representations for the given batch, serving as a critical indicator of the model's capacity to capture distinct features from the input data.

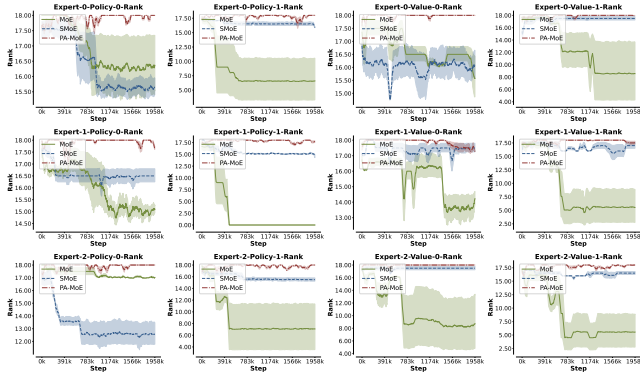


**Figure 12: Visualization results of the feature rank (Rank) across different layers of the policy and value networks for various experts.**

Figure 12 illustrates the evolution of feature rank across different experts under various algorithms. It is evident that our approach, PA-MoE, consistently maintains a higher rank, effectively mitigating the loss of plasticity.

## G Layer-wise Analysis of Expert Effective Rank in PA-MoE

To further understand the representational capacity of different models, we analyze the effective rank of hidden features across the network layers. The effective rank serves as a proxy for the diversity and richness of learned representations. By evaluating this metric, we gain insights into how well each method utilizes the available feature space.

**Definition G.1 (Effective Rank).** Let  $\{\sigma_i\}_{i=1}^n$  be the singular values of a matrix. Define the normalized singular values as  $p_i = \frac{|\sigma_i|}{\sum_{j=1}^n |\sigma_j|}$ . The Shannon entropy of these normalized values is computed as

$$H = - \sum_{i=1}^n p_i \log(p_i), \quad (43)$$

with the convention that  $0 \log 0 = 0$ . The effective rank is then defined as

$$r_{\text{eff}} = e^H. \quad (44)$$

This measure reflects the effective dimensionality of the matrix, capturing the spread and diversity of its singular value distribution.

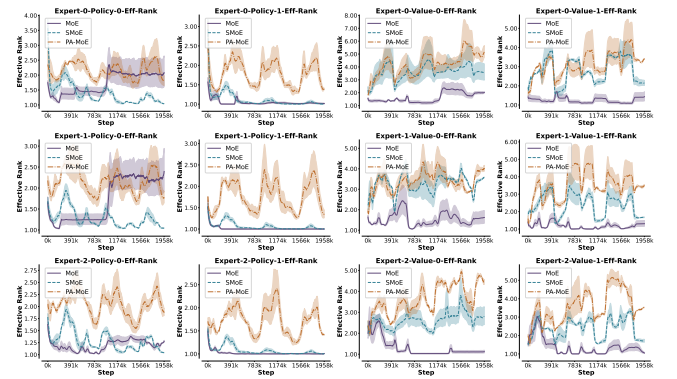


**Figure 13: Visualization results of the effective rank (Eff-Rank) across different layers of the policy and value networks for various experts.**

Figure 13 demonstrates that the effective rank of the features produced by our proposed method is consistently higher than that of other approaches. The effective rank quantifies the intrinsic dimensionality of the hidden representations by measuring the spread of the singular values. A higher effective rank indicates that our algorithm maintains a richer and more diverse feature space, thereby preserving model plasticity. This enhanced plasticity allows the model to adapt more effectively to varying conditions and capture a broader range of data characteristics, highlighting the superiority of our approach in maintaining robust and adaptable representations.

## H Layer-wise Analysis of Expert Approximate Rank in PA-MoE

To complement the insights provided by the effective rank, we further investigate the approximate rank of the learned representations across layers. While the effective rank captures entropy-based diversity, the approximate rank emphasizes variance concentration, offering a more interpretable view of how many principal directions contribute significantly to the overall feature space. This allows us to assess how compact yet expressive the representations are under different expert configurations.

**Definition H.1 (Approximate Rank).** Let  $\{\sigma_i\}_{i=1}^n$  be the singular values of the feature matrix  $M$ . The squared singular values  $\sigma_i^2$  represent the variance contributed by each singular direction. Normalize these values as

$$p_i = \frac{\sigma_i^2}{\sum_{j=1}^n \sigma_j^2}. \quad (45)$$

The approximate rank is defined as the smallest integer  $r$  such that the cumulative sum of the normalized squared singular values satisfies

$$\sum_{i=1}^r p_i \geq \text{prop}, \quad (46)$$

where  $\text{prop}$  is a predetermined threshold (typically 0.99). This metric quantifies the effective dimensionality of  $M$  by capturing the minimal number of singular components that account for a specified proportion of the total variance.

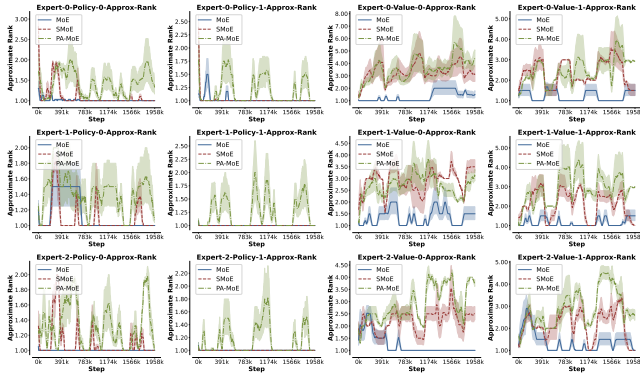


**Figure 14: Visualization results of the approximate rank (Approx-Rank) across different layers of the policy and value networks for various experts.**

Figure 14 shows that our proposed PA-MoE approach consistently achieves a higher approximate rank than other methods, reflecting its ability to capture a greater proportion of the feature variance and thereby better preserve model plasticity.

## I Layer-wise Analysis of Expert Approximate Absolute Rank in PA-MoE

Building upon the previous metrics, we introduce the absolute approximate rank to offer an alternative lens on representational

capacity. Unlike the traditional approximate rank—which is based on the squared singular values and thus biased toward variance concentration—this measure leverages the raw singular values, focusing instead on the cumulative magnitude of feature directions. As a result, it emphasizes the breadth of significant components rather than just the dominant ones. This shift provides a complementary understanding of how information is distributed across the spectrum of feature dimensions.

**Definition I.1 (Absolute Approximate Rank).** Let  $\{\sigma_i\}_{i=1}^n$  be the singular values of a matrix  $M$ . Instead of using squared singular values, we define the absolute approximate rank as the smallest integer  $r$  such that, when the singular values are sorted in descending order and normalized by their sum, the cumulative sum of the top  $r$  normalized singular values reaches or exceeds a specified threshold  $p$  (e.g., 0.99). Formally, if we define

$$p_i = \frac{\sigma_i}{\sum_{j=1}^n \sigma_j}, \quad (47)$$

with  $p_1 \geq p_2, \dots, \geq p_n$ , then the absolute approximate rank is given by

$$r_{\text{abs}} = \min \left\{ r \mid \sum_{i=1}^r p_i \geq p \right\}. \quad (48)$$

Unlike the standard approximate rank—which squares the singular values to emphasize their variance contribution—this metric evaluates the effective dimensionality based on the raw singular values, offering an alternative perspective on the matrix’s representational capacity.

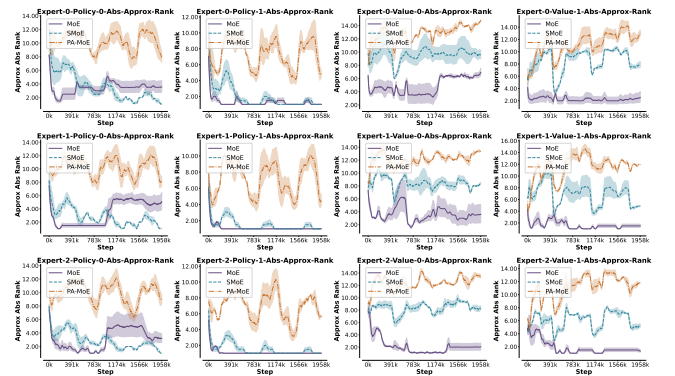


**Figure 15: Visualization results of the approximate absolute rank (Abs Approx-Rank) across different layers of the policy and value networks for various experts.**

Figure 15 illustrates that our PA-MoE approach consistently yields a higher absolute approximate rank compared to other methods. This superior rank, derived from the raw singular values, indicates that our method captures a broader and more nuanced spectrum of feature information. Consequently, this leads to richer and more diverse representations, which in turn preserve model plasticity. Ultimately, the elevated absolute approximate rank underscores the robustness and effectiveness of our approach in maintaining comprehensive and discriminative feature representations.

## J Visualization of Expert Weight Distribution in PA-MoE

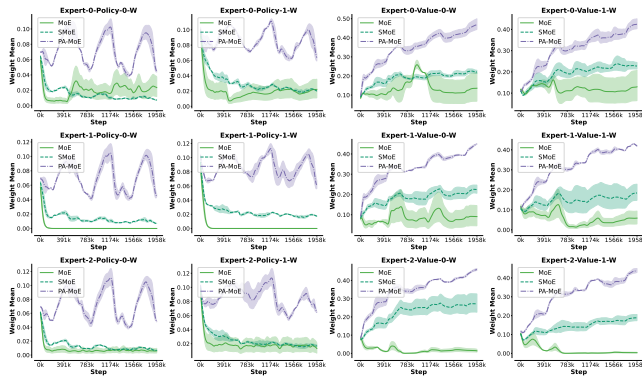


**Figure 16: Visualization results of the weight mean (W) across different layers of the policy and value networks for various experts.**

Figure 16 presents a visualization of the weight dynamics across different layers and experts under QoE shift scenarios. Compared to the baseline, PA-MoE consistently exhibits larger weight magnitudes. This phenomenon is attributed to the noise-injection-based forgetting mechanism: when critical information needs to be retained, the network responds by adaptively amplifying the corresponding weights, thereby counteracting the effects of noise-induced forgetting. This adaptive behavior enables PA-MoE to strike a dynamic balance between memory retention and forgetting, which is essential for maintaining plasticity in non-stationary environments.